Asian Journal of Chemistry Vol. 22, No. 8 (2010), 5902-5912

Crystallization Properties of Polycaprolactone Induced by Different Hydroxyapatite Nano-Particles

CHEN GUANG-MEI*, ZOU TIE-MEI, CHEN LEI and HUANG YI-PING†
School of Materials and Chemical Engineering, Anhui Institute of Architecture and Industry, Hefei, Anhui-230601, P.R. China
E-mail: chen_gm168@yahoo.com.cn

Polycaprolactone (PCL) composites were synthesized by two grades of hydroxyapatite (HA) nano-particles, namely, HA1 (prepared in our laboratory) and HA2 (purchased from commercial). The molar ratio of Ca/P for HA1 analyzed by ICP was 1.68 and 1.60 for HA2. The number average molecular weight of the polymers was measured by ^{1}H NMR. The crystallization behaviour of the samples was characterized by DSC, XRD and polarized light micrographs (PLM). The results indicated that polycaprolactone prepared by different HA nano-particles had slightly change in the number average molecular weight for the same content of HA. But the crystallization behaviour of the nano-HA/PCL samples had identical change tendency with the change of HA content in the samples. Both grades of HA nano-particles could increase the crystallization temperatures (T_c) of PCL from 25-28 °C, decrease the melting temperatures (T_m) from 61-55 °C and decrease the crystallinity of PCL from 55 to 39 %. When the content of nano-HA in the composites was 5 wt %, the thermal decomposition temperature could be elevated about 100 °C. The results for measurements suggested that the nano-HA/PCL composites with analogical properties could be obtained by the same content of HA either prepared in our laboratory or purchased from commercial.

Key Words: Polycaprolactone, Hydroxyapatite nano-particles, The composites, Crystallization behaviour.

INTRODUCTION

Hydroxyapatite (HA) is a commonly used ceramic in bone tissue engineering because of its excellent hard-tissue compatibility, bioactivity, osteoconductivity, non-toxicity, noninflammatory behaviour and nonimmunogenicity[1-3]. However, the pure HA has poor tensile strength and weak fatigue resistance in the humoral surrounding. Thus, in recent years, the composites of HA particles and biodegradable polymer were investigated by various methods. One of these is physically blending HA with the polymers such as poly(ε-caprolactone) (PCL), polyglycolide (PGA), polylactide (PLA) and their corresponding copolymers[4-6]. The composites exhibited good osteoconductivity, biodegradability and high mechanical strengths. But the HA particles were in lack of adhesion with the polymer matrix in the composites.

†School of Chemistry and Chemical Engineering, Anhui University, Hefei, Anhui, 230039, P.R. China.

The weak interfacial adhesion may result in the decrease of mechanical properties of the composites and the aggregation of the fillers, especially the HA nano-particles. So improvement of the interfacial adhesion between the HA particles and the polymer matrix has become very important in the studies on the composites. The other method which can improve the interfacial adhesion is the polymer directly grafted onto the hydroxyl group of the HA or modified HA[7-10]. It was reported that poly(L-lactide) (PLLA) was directly connected onto the surface of hydroxyapatite nano-particles by the grafting ring-opening polymerization of L-lactide. The HA nano-particles still retained the original dimension and shape. For another biodegradable polyester-poly(ε-caprolactone) (PCL), two methods have also been reported in some references[11-13]. But it was an issue that the nano-HA can be obtained in scores if the composites are applied practically. In these papers, nano-HA synthesis techniques include sol-gel methods, co-precipitation, emulsion techniques, mechanochemical methods, electrochemical deposition and hydrothermal processes. However, none of these methods are feasible for large-scale industrial production processes because they involve expensive materials, complicated processes, serious aggregation, synthesis steps include gelation, aging, drying and sintering. Up to now, the commercial HA nano-particles which are available commercially in low cost and conveniently might be processed from the natural organism, such as natural coral exoskeleton. The composition and size of the commercial HA nano-particles may influence the properties of the composites. In order to compare the effect of HA obtained by different methods on the composites, in the present work, HA nano-particles synthesized in our laboratory and obtained from the commercial product respectively were used to prepare the nano-HA/PCL composites. The samples were characterized by ^{1}H NMR, FTIR, DSC, XRD and PLM. The characterization results indicated that the properties of the composites prepared by different HA nano-particles exhibited slight difference.

EXPERIMENTAL

Calcium nitrate, ammonium hydrogen phosphate and stannous octoate were purchased commercially from Shanghai Reagent Co. and used without further purification. ε-Caprolactone (CL) was purchased from Aldrich Co. Prior to use, CL was dried over calcium hydride and vacuum distilled. Toluene was distilled from Na/benzophenone under N_2.

Synthesis of HA nano-particles: HA nano-particles were prepared by a hydrothermal technique according to the modified literature procedure[14]. First, 0.5 M $Ca(NO_3)_2$ solutions and 0.3 M $(NH_4)_2HPO_4$ solutions were obtained by dissolving $Ca(NO_3)_2{\cdot}4H_2O$ and $(NH_4)_2HPO_4$ in distilled water, respectively and the pH of each solution was adjusted to 10-11 with ammonia solution (25 %). The solution of $(NH_4)_2HPO_4$ was added drop-wise into the $Ca(NO_3)_2$ solution (v/v = 1:1) under mechanical stirring to obtain a slurry and the pH of the slurry was maintained at pH 10-11 using ammonia solution (25 %). The obtained slurry was transferred into stainless steel autoclaves and heated at 130 °C for 12 h and then cooled to room

temperature naturally. After hydrothermal process, the HA nano-particles were washed with distilled water *via* centrifugation until the pH value approached 7. The resultant powder was dried at 60 °C for 48 h. The final product, HA nano-particles, was obtained by heating at 700 °C for 3 h. The HA nano-particles were rod crystals of about 100 nm in length and 10-20 nm in width (XRD) (marked HA1). On the other hand, commercial HA nano-particles were also rod crystals of about 180 nm in length and 20-50 nm in width tested by TEM (marked HA2). The chemical composition of the particles was determined by a Seiko induced coupled plasma (ICP) spectrometer. The samples for the ICP analysis were dissolved in a 1 mol dm^{-3} HNO_3 solution[15]. The molar ratio of Ca/P for HA1 is 1.68 and 1.60 for HA2.

Graft polymerization of CL on HA nano-particles: A suspension of HA in 5-10 mL dry toluene was heated at reflux using a Dean-Stark apparatus for 12 h. At room temperature, 20 g CL and 0.5 g $Sn(Oct)_2$ were added under nitrogen. The temperature was then raised to 140 °C. The reaction was maintained for 12 h. The product was diluted with methylene chloride and the HA particles were separated by a repeated washing-centrifugation cycle at 2500 rpm for 10 min. The actual content of nano-HA existed in the molecule chains can be calculated and showed in Table-1.

TABLE-1
CONTENT OF HA IN RAW MATERIALS AND COMPOSITES

Samples	HA1 wt %		Samples	HA2 wt %	
	In raw materials*	In composites**		In raw materials*	In composites**
HP11	1	1.00	HP21	1	1.00
HP12	3	2.98	HP22	3	2.95
HP13	5	4.85	HP23	5	4.80
HP14	7	6.60	HP24	7	6.68
HP15	10	8.96	HP25	10	8.53
HP16	20	13.78	HP26	20	13.29

*Nano-HA content in the raw materials. **Nano-HA content in the composites through centrifugation separation.

Measurement

Molecular weight of the polymers: The number-average molecular weight (Mn) of the polymers was evaluated by ^1H NMR using end-group analysis. Measurements of ^1H spectra were conducted in $CDCl_3$ solution under ambient temperature on an AM 300 FT Bruker spectrometer using tetramethyl silane (TMS) as internal standard.

Transmission electron microscopy: TEM (Jeol JEM-1010) was used to determine the size and shape of the HA nano-particles in the composites. For TEM observation, ultra thin sections (with thickness of about 100 nm) were prepared at -60 °C with a Leica ultramicrotome using a diamond knife.

Fourier transmission infrared spectrum: FTIR spectra were obtained using a NEXUS 870 FT-IR instrument. Thin films of all samples were cast on KBr windows from 0.5 % (w/v) tetrahydrofuran solutions. After most of the solvent was evaporated at room temperature, the films were transferred to a vacuum oven and kept at 60 °C for 1 week to remove residual solvent. All spectra were recorded at room temperature and at a resolution of 2 cm^{-1} after 32 scans, signal averaged.

DSC: Melting and crystallization behaviour for the nano-HA/PCL were studied by DSC using a Perkin-Elmer Pyris-1 apparatus. The samples were heated from 20-100 °C for the first scan at 20 °C/min and maintained at 100 °C for 5 min. The composites were cooled down to -20 °C at a rate of 20 °C/min and kept at this temperature for 1 min. Subsequently, the samples were heated again from -20-100 °C for the second scan. A heating rate of 20 °C/min was used. The melting point (T_m) and the crystallization point (T_c) of each sample were located in the maximum of their respective peaks.

XRD: All wide-angle X-ray diffraction measurements were obtained at ambient temperature on a MXP18AHF X-ray diffractometer using Cu K_α radiation (40 mA, 40 kV). The 2θ range was from 10-40° at a scanning speed of 0.5°/min. Samples for wide angle X-ray diffraction were injection molded under nitrogen at 100 °C and transferred at ambient temperature to a circular mold with a diameter of 20 mm and a thickness of 1 mm.

Optical microscopy: The crystallization of the PCL in the composites was investigated by a polarized light microscope with a hot stage. The samples were heated for 5 min at 100 °C and isothermally crystallized at the crystallization temperature T_c = 33, 36, 39 and 42 °C, respectively. Photographs of the samples were taken.

TGA: To determine the stabilization temperature, thermogravimetric analyses (TGA) of the samples were carried out using a Pyris1 TGA (PE Crop. USA). The sample powder was heated at 10 °C/min from 20-500 °C under nitrogen.

RESULTS AND DISCUSSION

The number-average molecular weight: The molecular weight of the polymers was characterized by ^{1}H NMR.

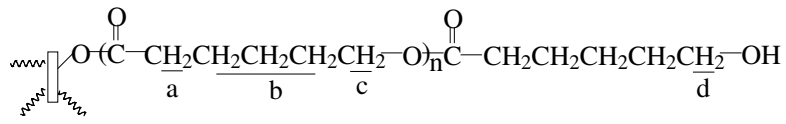

HA

Signals in the ^{1}H NMR of the composites appeared at δ: 4.06 (Hc), 2.31 (Ha), 1.66, 1.39 (Hb) and 3.63 (Hd). According to the peak areas of the signals, the molecular weight of the PCL can be calculated, shown as the eqns. 1 and 2:

$$\frac{A_d}{A_a} = \frac{2}{2(n+1)} \quad (1)$$

$$W_{PCL} = 114(n+1)+1 \quad (2)$$

where A_d and A_a are the peak areas for the H_d and H_a, respectively. The results of W_{PCL} are shown in Fig. 1.

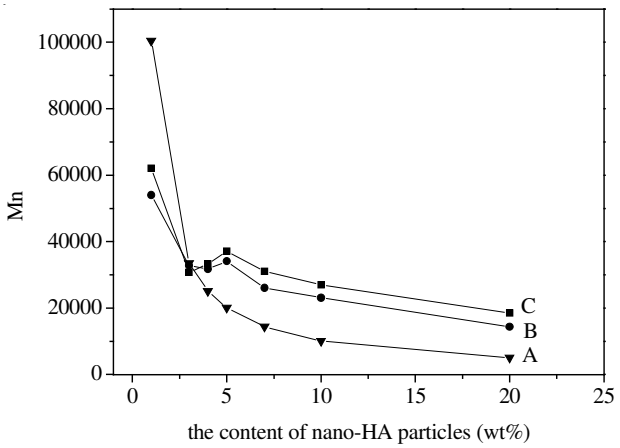

Fig. 1. Number average molecular weight of the composites variety traces with the content of nano-HA particles. (A) the theoretic value; (B) HA1/PCL; (C) HA2/PCL

In Fig. 1, it can be seen that the molecular weight of the PCL decreases with the increase of nano-HA, either synthesized or purchased. In order to evaluate this result, the theoretical value of the molecular weight of the PCL was estimated as shown in eqn. 3 and also shown in Fig. 1.

$$W_{tPCL} = \frac{m_1}{2(m_2/1004)} \quad (3)$$

where m_1 and m_2 are the mass of ε-caprolactone and hydroxyapatite in the raw materials put into the reactor, respectively. Because ε-caprolactone can be induced only by OH groups on the surface of HA nano-particles, W_{PCL} should be larger than the W_{tPCL}.

From Fig. 1, when the content of HA in the composites was 1 wt % the result by measurement was lower than that of the theoretical values. But when the content of nano-HA was higher than 5 wt %, the measurement results were higher than those of the theoretical values. In the low HA content, less caprolactone monomers were ring-opening polymerized directly on exterior hydroxyl groups of HA particles and formed higher molecular weight PCL finally. In the reaction system, because of a small quantity of dry toluene, the higher molecular weight PCL leads to the higher viscosity of the system. In the higher viscosity, CL molecule transfers to the reaction interface difficultly. So in the end some CL monomers can not be grafted and the actual molecular weight of PCL is lower than the theoretical value. When nano-HA content increases to 5 wt %, some HA particles will be aggregated in the polymerization although the nano-HA has been dispersed in the monomers

adequately. The aggregated HA nano-particles increase with the increasing of the HA content in the system, especially when the content of nano-HA are above 5 wt %, as pointed out in Table-1. The partial exterior hydroxyl groups of HA particles can not induce the CL ring-opening polymerization when the aggregated HA nano-particles form. The actual molecular weight of PCL is higher than the theoretical value. In the Fig. 1, it can also be seen when the content of HA more than 5 wt % the molecular weight of the composites synthesized by HA2 is higher than that of the samples by HA1 at same HA content. It can be deduced from the size of the HA nano-particles. HA2 has a bigger average size than HA1.

Transmission electron microscopy (TEM): Fig. 2 shows the TEM images for the HA1, HA2 and the composite HP23. The morphologies of HA1 and HA2 are similar rod although the size has obvious difference. In HP23, a spot of aggregated HA nano-particles can be observed although the nano-HA has been dispersed in the monomers adequately. The results display that it is very different to prevent the aggregation of the higher content HA nano-particles in the composites. When the content of HA is above 5 wt % some of the HA nano-particles are not homogeneously dispersed. It can also confirm the change of the composites' molecular weight with the HA content in the front section.

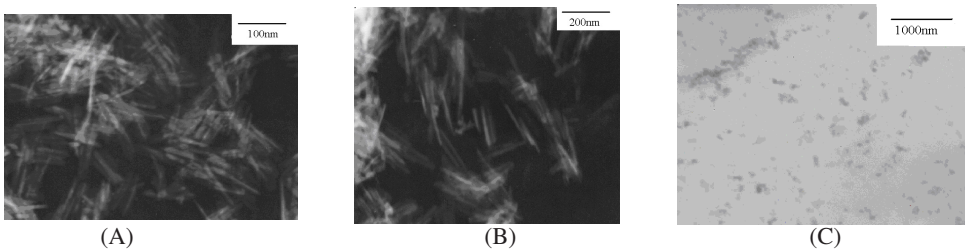

(A) (B) (C)

Fig. 2. TEM images for the samples. (A) HA1; (B) HA2; (C) HP23

Fourier transmission infrared spectra (FTIR): FTIR spectra of the samples are shown in Fig. 3. For HA nano-particles, band characteristics of PO_4^{3-} appear at 472, 563, 601, 961 and 1033 cm^{-1}. The broad and high intensity bond extending from 3700-3100 cm^{-1} and the band at 1623 cm^{-1} are the reflections of absorbed and combined water. On the other hand, sharp peak at 3573 cm^{-1} corresponds to the stretching vibration of OH^- ions, whereas the weak peak at 632 cm^{-1} is attributed to O-H vibrational mode. For HA2, the weak peaks at 1480 and 895 cm^{-1} bands are ascribed to CO_3^{2-}. It is obvious that the commercial HA nano-particles include more carbonates. So it can be understood that the molar ratio of Ca/P for HA1 is near to theoretical value and only 1.60 for HA2. In Fig. 3, it can be seen that the maximum carbonyl absorbance peak for PCL is at 1724 cm^{-1}. When HA content increases, the maximum carbonyl absorbance peak for the composites shifts to higher frequency slightly at 1726 cm^{-1}. As pointed out by Coleman *et al.*[16], the bands at 1722 and 1737 cm^{-1} for pure PCL represent the crystalline and amorphous phases, respectively. So the carbonyl absorbance peak for the composites at 1726 cm^{-1} indicates

that HA particles play a negative effect to the crystallinity of the PCL. However, the carbonyl absorbance peak for the HA/PCL samples do not change with the HA content in the samples. Obviously, the degree of crystallinity of PCL in the samples keep no change with the increasing of the HA content when HA is less than 20 %. From the HP13 and HP23 in the Fig. 3, it can be seen that the IR spectra for different HA nano-particles have same results.

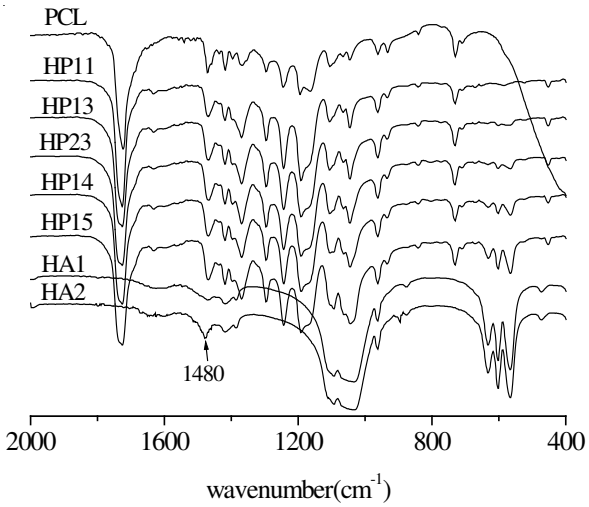

Fig. 3. FTIR spectra of the samples at the range from 2000-400 cm^{-1}

X-Ray diffraction: Fig. 4 shows the XRD patterns for the specimens PCL, HA1, HP11, HP13, HP15 and HP23, respectively. Several PCL peaks with a broad halo peak were observed to occur because PCL had semi-crystalline structure. The peaks found at around 21.5, 22.1 and 23.8° were assigned to (110), (111) and (200) planes of the PCL and a broad halo peak is likely to come from the amorphous

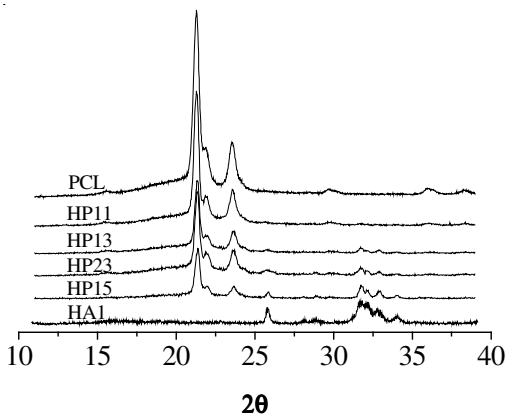

Fig. 4. Ambient temperature X-ray diffractograms of some composites

region of PCL. XRD Patterns of the composites show the presence of two phases: polymeric and nano-particles. In polymeric part, as the PCL content in the composites increased, the peak of PCL increased slightly indicating good crystallinity for PCL. On the other hand, a poor crystalline part consisting of characteristic broad diffraction maximum at 2θ about 25.8° and 31.7° are identified as hydroxyapatite. In Fig. 4, it can be seen that the composites include HA1 and HA2 have analogical morphology.

DSC and TGA: The crystallization temperatures (T_c), the melting temperatures (T_m) and fusion enthalpy (ΔH_f) of the samples, measured in the second heating cycle, are summarized in the Table-2 as a function of the weight fraction of HA content. Table-2 shows that pure PCL has a lowest T_c and a highest T_m. When nano-HA particles are put into the composites the T_c increases to about 28 °C and T_m decreases from 61 to 55 °C.

TABLE-2
CRYSTALLIZATION AND FUSION PARAMETERS FOR THE COMPOSITES

Samples	T_m (ºC)	T_c (ºC)	ΔH_f (J g^{-1})	Cr (%)
PCL	61.2	24.8	74.66	55.1
HP11	57.2	27.8	61.84	46.1
HP12	57.6	27.5	61.67	46.9
HP13	57.0	28.1	58.49	45.4
HP14	56.8	27.8	56.57	44.7
HP15	57.2	27.4	54.02	43.6
HP16	54.9	26.8	46.50	39.8
HP21	56.9	28.0	61.90	46.1
HP22	57.4	27.6	60.89	46.3
HP23	57.1	27.8	58.42	45.3
HP24	57.6	27.5	55.89	44.2
HP25	57.2	27.6	54.31	43.8
HP26	55.4	26.3	44.76	38.1

At the same time, the fusion enthalpy also decreases obviously from 74.66-62.45 J/g. It is well-known the crystallinity (Cr), of the PCL can be calculated from the enthalpy of melting (ΔH_f) by eqn. 3:

$$Cr = [\Delta H_f/(W_{PCL} \times \Delta H_f^0)] \times 100\ \% \quad (3)$$

where W_{PCL} = weight fraction of PCL in composites and ΔH_f^0 = 135.5 J/g is the reference melting enthalpy of 100 % crystalline PCL[17]. The crystallinity of the pure PCL reaches a value of about 55 % in the second scan. But in the composites the crystallinity of PCL is about 44-46 %. In Table-2, it can be seen that T_c, T_m and crystallinity for PCL in the composites are nearly no change with the content of HA. These results indicated that nano-HA particles can change the crystallization behaviour of PCL obviously, but the effect of the HA content on the crystallization behaviour of PCL can't be observed in present investigation range.

Fig. 5 gives the TGA curves of the composites. When the content of HA is below 5 wt % the decomposition temperatures (T_d) for the composites increase

with increasing of HA. The highest T_d appears at containing 5 wt % nano-HA, either for HA1 or for HA2. Obviously, the composites with 5 wt % nano-HA particles have the best thermal stabilization. Pure PCL has a decomposition temperature at about 340 °C (the maximum value of their respective derivative thermogravimetry peaks), but the highest decomposition temperature for the composites is about 435 °C.

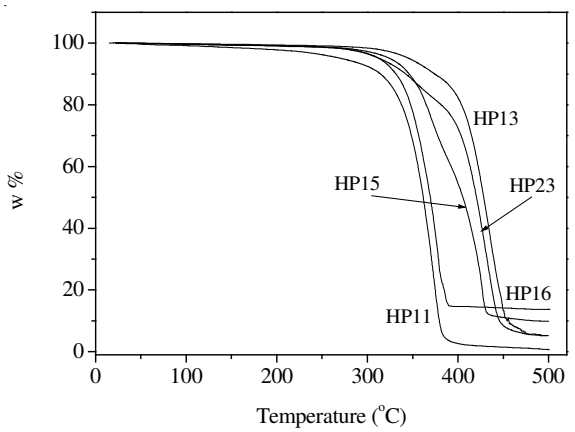

Fig. 5. TGA traces of some samples recorded at the heating rates 10 °C/min

Polarized light micrographs (PLM): Fig. 6 shows the optical micrographs viewed with cross polars for some specimens obtained at 39 °C for 72 h after cooling

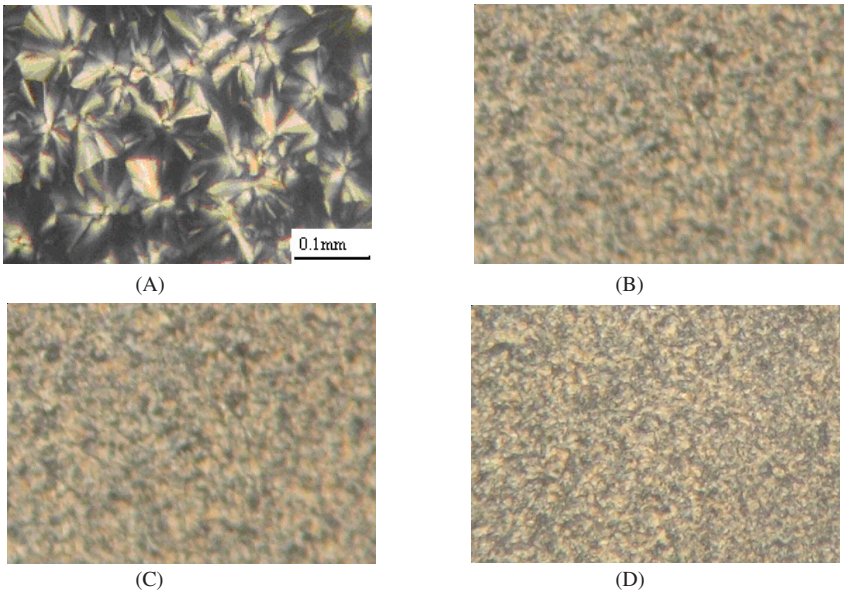

Fig. 6. Polarized light micrographs of the samples obtained at 39 °C for 72 h. (A) PCL; (B) HP12; (C) HP13; (D) HP23

from the molten state. It is obvious to see that the larger spherulitic dimensions on the order of about 80 μm are observed for pure PCL. Much smaller spherulitic dimensions appear in the composites that contain nano-HA. In the micrograph of the sample HP12, we only can observe large numbers of spots not more than 5 μm in diameters. Optical micrographs reveal that the some composites crystallites are birefringent but not clear spherulitic as shown in Fig. 6(C), although an increase in the nucleation density can be observed in this sample. It indicates that nano-HA particles are effective nucleating points for PCL. So it can be seen in Fig. 6, when the content of HA is below 5 wt % the nucleation density increases and the spherulitic dimension decreases for PCL crystal with the increasing of HA in the composites. Because of the bigger size, HP23 has larger spherulitic dimensions than that of HP13, although they have equivalent nano-particles. In fact, the crystallization morphologies of the samples crystallized at 33, 36 and 42 °C have similar rule with these at 39 °C. Summarized the results of FTIR, XRD, DSC and PLM, induced synthesis from HA nano-particles, the crystallization behaviour of PCL can be affected by the nano-particles obviously. But the property difference of PCL contributed to the different HA nano-particles is feebleness.

Conclusion

In the present work, two grades hydroxyapatite nano-particles, one synthesized in our laboratory and the other purchased commercially, are used to induce the ring-opening polymerization for caprolactone monomer. Because the polymer directly grafted onto the surface hydroxyl groups of HA, the HA nano-particles can be dispersed in the monomers adequately when the content of nano-HA is below 5 wt %. The accession of nano-HA by grafted on the polymer can influence the crystallization behaviour of PCL obviously. The crystallinity decreases, the crystallization temperatures (T_c) increase and the melting temperatures (T_m) decrease. On the other hand, the thermal stabilization of the composites arrive the highest when the content of nano-HA particles is 5 wt %. It can be guessed the composites containing 5 wt % nano-HA have some prominent properties.

In above-mentioned, it is not worthy that the effect of the commercial nano-HA particles on the crystallization behaviour of the PCL is consistent with the nnao-HA particles made in our laboratory. Obviously, the nano-HA/PCL composites with analogical properties can be obtained by either HA1 or HA2, except the spherulitic dimensions due to the bigger size of the HA2.

ACKNOWLEDGEMENTS

The authors gratefully acknowledged the support of Natural Science Fund of Anhui Province (Grant Number 070414193), Anhui Key Laboratory of Advanced Building Materials and the fund K02384.

REFERENCES

1. R.Z. LeGeros, Calcium Phosphates in Oral Biology and Medicine, Karger: Basel, Switzerland (1991).
2. H. Aoki, M. Akao, Y. Shin, T. Tsuji and T. Togawa, *Med. Prog. Tech*., **12**, 213 (1987).
3. O. Kilian, S. Wenisch, S. Karnati, E. Baumgart-Vogt, A. Hild, R. Fuhrmann, T. Jonuleit, E. Dingeldein, R. Schnettler and R.-P. Franke, *Biomaterials*, **29**, 3429 (2008).
4. S.C. Wong, B. Avinash and N.G. Alan, *Comp. A: Appl. Sci. Manufac.*, **39**, 579 (2008).
5. Z. Hong, X. Qiu, J. Sun, M. Deng, X. Chen and X. Jing, *Polymer*, **45**, 6699 (2004).
6. I. Nenad and U. Dragan, *Appl. Surface Sci*., **238**, 314 (2004).
7. N.D. Luong, I.-S. Moon, D.S. Lee, Y.-K. Lee and J.-D. Nam, *Mater. Sci. Eng. C*, **28**, 1242 (2008).
8. R.E. Neuendorf, E. Saiz, A.P. Tomsia and R.O. Ritchie, *Acta Biomater*., **4**, 1288 (2008).
9. J.L. Hong, W.C. Hyung, J.K. Kyung and C.L. Sang, *Chem. Mater*., **18**, 5111 (2006).
10. L. Qing, R.W. Joost, G. Klaas and A.B. Clemens, *Biomaterials*, **19**, 1067 (1998).
11. H.W. Kim, C.K. Jonathan and H.E. Kim, *Biomaterials*, **25**, 1279 (2004).
12. S. Lauren, G. Selcuk, X.J. Wen, G. Milind and W. Sun, *Biomaterials*, **28**, 5291 (2007).
13. H.J. Lee, S.E. Kim, H.W. Choi, C.W. Kim, K.J. Kim and S.C. Lee, *Eur. Polym. J*., **43**, 1602 (2007).
14. W.L. Suchanek, K. Byrappa, P. Shuk, R.E. Riman, V.F. Janas and K.S. TenHuisen, *Biomaterials*, **25**, 4647 (2004).
15. T. Ishikawa, A. Teramachi, H. Tanaka, A. Yasukawa and K. Kandori, *Langmuir*, **16**, 10221 (2000).
16. M.M. Coleman and J. Zarian, *J. Polym. Sci. Polym. Phys. Ed*., **17**, 837 (1979).
17. V. Grescenzi, G. Manzini, G. Calzolari and C. Borri, *Eur. Polym. J.*, **8**, 449 (1972).

(*Received*: 25 August 2009; *Accepted*: 28 April 2010) AJC-8639